Jürgen Ulpts, Wolfgang Dreher, Lars Kiewidt, Miriam Schubert, Jorg Thöming

In situ analysis of gas phase reaction processes within monolithic catalyst supports by applying NMR imaging methods

Journal Article	as:	peer-reviewed accepted version (Postprint)
DOI of this document*(secondary publication):		https://doi.org/10.26092/elib/2460
Publication date of this document:		11/09/2023

* for better findability or for reliable citation

Recommended Citation (primary publication/Version of Record) incl. DOI:

Jürgen Ulpts, Wolfgang Dreher, Lars Kiewidt, Miriam Schubert, Jorg Thöming,
In situ analysis of gas phase reaction processes within monolithic catalyst supports by applying NMR imaging methods,
Catalysis Today, Volume 273, 2016, Pages 91-98, ISSN 0920-5861,
https://doi.org/10.1016/j.cattod.2016.02.062

In situ analysis of gas phase reaction processes within monolithic catalyst supports by applying NMR imaging methods

Jürgen Ulpts[a,*], Wolfgang Dreher[b], Lars Kiewidt[a], Miriam Schubert[a], Jorg Thöming[a]

[a] Center for Environmental Research and Sustainable Technology (UFT), University of Bremen, Leobener Straße, 28359 Bremen, Germany
[b] In vivo MR group, Department of Chemistry (FB 2), University of Bremen, 28359 Bremen, Germany

ARTICLE INFO

Article history:
Received 11 December 2015
Received in revised form 8 February 2016
Accepted 10 February 2016
Available online 29 March 2016

Keywords:
3D magnetic resonance spectroscopic imaging
Catalytic monolith
Gas phase reaction
Non-invasive concentration measurement

ABSTRACT

Measuring spatially resolved concentration distributions in gas phase reaction systems is an important tool to validate simulation calculations, improve the understanding of transport processes within the catalyst, and identify potentials for improvements of monolithic catalyst supports. The commonly used measurement methods for such opaque systems are invasive and, thus, might be misleading due to alteration of the system.

To overcome this issue, a 3D magnetic resonance spectroscopic imaging (MRSI) method was developed and implemented on a 7-Tesla NMR imaging system to map the concentration distributions within opaque monolithic catalysts using the ethylene hydrogenation process as case study. The reaction was catalyzed by a coated sponge packing or a honeycomb monolith within an NMR compatible packed bed reactor. Temperatures at the inlet and the outlet of the catalyst beds were simultaneously determined by analyzing the spectra of inserted ethylene glycol filled glass capsules. Steady state concentration profiles and temperature levels were measured at different reaction conditions. In order to prove the plausibility of the measured spatial distributions of compound concentrations, the experimental results were compared to a 1D model of the reactor based on kinetic data from literature. Furthermore, a comparison with integral concentration measurements using a mass spectrometer demonstrated deviations below 5%. The results show that 3D MRSI is a valuable and reliable tool to non-invasively measure spatially resolved process parameters within optically and/or mechanically inaccessible structured monolithic catalyst supports, even if only standard thermal polarization is exploited and the use of expensive and technically challenging signal enhancement techniques (hyperpolarization) is avoided. We expect that 3D MRSI can pave the way toward deeper insight into the interactions between catalyst, catalyst support, and gas phase.

1. Introduction

Within the last decades structured catalyst supports became a valuable option to enhance the performance of heterogeneously catalyzed reaction processes. Their beneficial properties, like low pressure drop and adjustable heat transport characteristics, are especially suitable to intensify gas phase reaction processes with elevated exothermicity [1–3]. Despite the wide application of monolithic catalysts in environmental catalysis, reliable and validated reactor models are still necessary to identify enhancement potentials when applying structured catalysts. However, the validation of modeling approaches of reaction systems with structured catalyst supports is still challenging due to the typically inaccessible and opaque nature of these supports, which makes non-invasive measurements of temperature and chemical concentration of the reactive flow within the catalyst bed rather difficult.

Although invasive methods such as suction probe techniques and thermometers provide only low spatial resolution and might lead to significant increase of the local residence time when applied for monolithic catalysts [4], they are still state-of-the-art and frequently applied in current research [3,5,6]. Another approach to map chemical compositions and temperature non-invasively, particularly in optically opaque reaction systems, are nuclear magnetic resonance (NMR) based methods, which are well established in biomedical diagnostics and analytical chemistry, and have also found various applications in material sciences and chemical engineering [7]. Several studies on investigating 3-phase reaction systems [8–10] with NMR techniques have been published, in

* Corresponding author.
E-mail address: julpts@uni-bremen.de (J. Ulpts).

which signal detection was mainly based on the liquid phase. Also gas phase processes have been investigated by NMR imaging and spectroscopy. In addition to the general difficulties associated with NMR measurements, like low inherent sensitivity and the required NMR compatibility of the reactor, the low spin density and rather short transverse relaxation times of gases make such measurements particularly challenging [11,12]. To overcome this issue, signal enhancement can be achieved by para-hydrogen induced hyperpolarization [13,14] or remote detection techniques [15,16], which are of particular interest for microreactors and systems with rather short residence times of the gas molecules. However, macroscopic reaction systems can also be investigated by using thermal polarization and standard volume radiofrequency (RF) coils, as recently demonstrated by applying ultrashort echo time multislice magnetic resonance spectroscopic imaging (MRSI). In that study a gas phase hydrogenation was characterized in a packed bed flow reactor containing Pt-Al_2O_3 pellets [17].

In this study, we demonstrate that MRSI can be successfully applied to look inside ceramic monolithic catalysts of macroscopic scale (Ø > 20 mm) under reaction conditions. We show how NMR measurements can help to understand the influence of the monolithic catalyst support on heat and mass transport in a gas phase process. To this end, we optimized and applied a 3D MRSI method. This approach allowed to measure both the spatial distribution of the reactants and products within two different monolithic catalyst supports using the ethylene hydrogenation as a model reaction, and the temperature at the inlet and outlet of the reaction zone. Furthermore, the experimental results are compared to predictions of a 1D model of the reactor.

2. Experimental

2.1. Materials

Three stacked γ-Al_2O_3-sponge segments (length: ~20 mm front and back segment and ~10 mm central segment (cf. Fig. 1a), diameter: 25 mm, 10 PPI; open porosity: 81%, Drache GmbH, Diez, Germany) and a cordierite honeycomb monolith (length: 50 mm, diameter: 25 mm, 600 cpsi, NGK, Poland) were used as monolithic catalyst supports.

All monoliths were coated with a 1 wt.% Pt/Al_2O_3 catalyst layer. To this end, tetraammineplatinum(II) chloride hydrate (Sigma-Aldrich, St. Louis, USA) was dissolved in water and mixed with an aqueous suspension containing γ-Al_2O_3 (BASF Catalyst Germany GmbH, Nienburg). After stirring the suspension for about 5 min, the monoliths were dipped into the suspension. Then, excessive material was blown off with compressed air. All samples were dried first at 120 °C and then at 490 °C, each for 3 h. The amount of catalytic material coated on the surface of the catalyst substrates was determined by weighting the substrates before and after coating and calcinating: The amount of coating material was approximately 1.6 g at the sponge segments and about 1.5 g at the honeycomb monolith. Prior to the experiments, the catalysts were activated using a gas flow of 2.5 Nl/min (H_2:N_2 1:5) at a temperature of 400 °C for about 2 h.

2.2. Ethylene hydrogenation

The reaction of choice was the exothermal hydrogenation of ethylene ($\Delta H_R = -137$ kJ/mol at 298 K) because it can be operated at ambient conditions, it selectively yields a single product (ethane), and, due to the symmetry of ethylene and ethane, both gases give rise to single resonance lines in ^{1}H NMR spectra. In addition, the chemical shift difference between the two signals is larger than 4 ppm [18], which facilitates signal separation. Furthermore, the availability of a broad set of kinetic data [19–21] for the Pt catalyzed ethylene hydrogenation allows the formulation of a simple rate expression which should meet a good level of accuracy for the applied reaction conditions (cf. Section 2.4).

The hydrogenation reaction was carried out within an NMR compatible glass reactor, which was cooled with pressurized air. The measurement range was arranged as follows (cf. Fig. 2): For constraining the reactive zone to a given area without any bypass flows or dead zones, the catalytic monoliths were tightly fitted into a glass tube (inner diameter: 25 mm; wall thickness: 1.5 mm length: 51 mm). The tube containing the catalytic monolith was in turn positioned inside the NMR compatible reactor. The resulting gap between glass tube and inner reactor wall was sealed with glass fiber sealing cord.

To measure the temperature at reproducible positions at the inlet and the outlet, ethylene glycol filled glass capsules were inserted into uncoated honeycomb segments (Ø 25 mm; length 25 mm; 600 cpsi), which were placed in front of and behind the catalytic monolith. Details of this temperature measurement method were described in a previous study [17]. To avoid flow disturbances and crosstalk of the ethylene glycol signal into the reactive zones, a gap of about 3 mm was left between the uncoated honeycomb segments and the catalytic monolith.

The process conditions were kept comparable to earlier ethylene hydrogenation studies [17]: The reactant gas supply of the reactor with argon, hydrogen and ethylene was realized by mass flow controllers (F-201CV, Bronkhorst, Ruurlo, Netherlands, FMA-2618-A, Omega Engineering, Stamford, USA).

To explore the limits of the 3D MRSI method, the total initial volume flow was set to either about 0.4 Nl/min or 1.0 Nl/min with different hydrogen content in the reactant gases. The corresponding experiments are referred to as “low flow rate experiment” and “high flow rate experiment” in the following text (cf. Table 1). The outlet pressure was held at a constant level of 1.3 bar (abs). Behind the reactor outlet, the composition of the product gases was analyzed by a process mass spectrometer (pMS, GAM 200, InProcess Instruments, Bremen, Germany).

Prior to the studies, the process mass spectrometer was calibrated with test gases manufactured by Linde (Ar:H_2, Ar:C_2H_4, Ar:C_2H_6; each 90 vol.%: 10 vol.% with regard to standard conditions, relative measurement uncertainty: 2%), leading to an accuracy better than 0.5 vol.%. Significant cross sensitivities between the different gases were not noticed during the calibration measurements.

2.3. MRSI experiments

All NMR experiments were performed on a 7 Tesla preclinical NMR imaging system (Biospec 70/20, Bruker Biospin GmbH, Etlingen, Germany) equipped with a magnetic field gradient system BGA12S2 with a maximum gradient strength of 441 mT/m per direction (x–z) and a rise time of 130 μs. A circularly polarized RF coil with an inner diameter of 72 mm was used for both RF transmission and signal detection.

Based on the multislice MRSI pulse sequence used in a previous study [17], a 3D MRSI sequence was developed and then applied with the following parameters: repetition time TR = 12.5 ms; flip angle: 15°, echo time TE = 0.35 ms; spectral width: 25 kHz; 256 complex data points per acquired time domain signal; matrix size for a non-isotropic spatial resolution (in x,y,z): $63 \times 63 \times 49$ with elliptically reduced phase encoding; field-of-view (FOV): $63 \times 63 \times 105$ mm^3; The slice thickness in z direction was adjusted to the FOV. The total measurement time was about 20.1 min and every measurement was repeated three times. Note that the short echo time, i.e., the delay between RF excitation and the start of data acquisition was achieved by using an optimized asymmetric

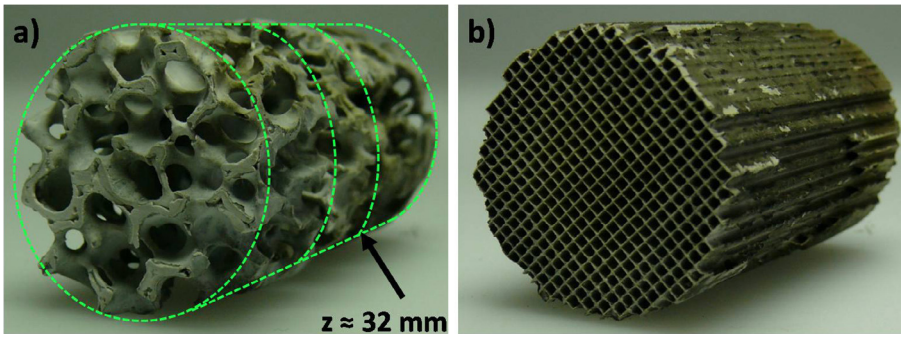

Fig. 1. (a) The monolithic sponge packing used in the first set of experiments consisted of three stacked 10 PPI sponge segments with 25 mm diameter and 20 mm (front and back segment) resp. 10 mm (central segment) length; the green dotted lines indicate the positions of the segments. The arrow indicates the position of the sponge cross section shown in Fig. 4a. (b) Picture of the coated cordierite honeycomb monolith (600 cpsi) used in the second set of experiments. (For interpretation of the references to colour in this figure legend, the reader is referred to the web version of this article).

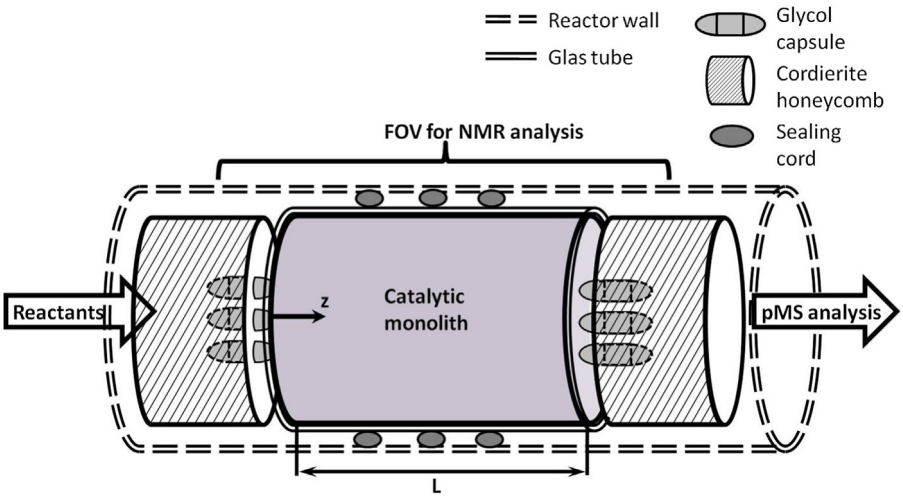

Fig. 2. Scheme of the experimental setup. The flow direction was from left to right.

Table 1
Experimental parameters (volume flow, concentration, temperature, velocity) of the low and high flow rate experiments on the sponge packing and the honeycomb. The volumetric concentrations were measured with a pMS behind the outlet of the reactor. The concentration measurements were performed at steady state conditions. For all experiments the measurement uncertainty of the pMS was below 0.5%. The measurement uncertainty of the temperature measurements derived from the ethylene glycol spectra and was below 1.5 °C.

	Low flow rate experiment (sponge)	High flow rate experiment (sponge)	Low flow rate experiment (honeycomb)	High flow rate experiment (Honeycomb)
Inlet:				
$\dot{v}_{Ar}$ in Nl/min	0.175	0.40	0.175	0.40
$\dot{v}_{C_2H_4}$ in Nl/min	0.22	0.50	0.25	0.50
$\dot{v}_{H_2}$ in Nl/min	0.078	0.10	0.075	0.10
Linear velocity in cm/s	1.6	3.4	1.7	3.4
T in °C (rotational axis)	56	32	50	32
Outlet:				
c_{Ar} in vol.%	41.6	44.0	41.8	44.4
$c_{C_2H_4}$ in vol.%	39.6	44.3	39.4	43.9
$c_{C_2H_6}$ in vol.%	18.0	11.0	18.0	11.0
c_{H_2} in vol.%	0.8	0.7	0.8	0.7
T in °C (on rotational axis)	65	117	61	106

RF pulse and a short duration of phase encoding of 260 μs in all three directions.

For visual inspection, data processing consisted of apodization (multiplication) of the measured raw data using a Hamming function followed by a 4D Fast Fourier Transform (FFT) and magnitude calculation.

For quantitative data evaluation, data fitting was performed using the matrix pencil method (MPM) [22–24,17], which approximates the measured time domain data by a sum of exponentially decaying signals each being defined by four parameters (amplitude, frequency, phase, decay constant). To this end, apodization and a 3D FFT in three spatial directions was performed followed by MPM fitting of the time domain data in each voxel (cf. Fig. 3). The performance of MPM for quantifying noisy spectroscopic NMR time domain data was investigated in [23] and [24], emphasizing the excellent estimation accuracy and the low "breakdown" signal-to-noise (SNR) threshold.

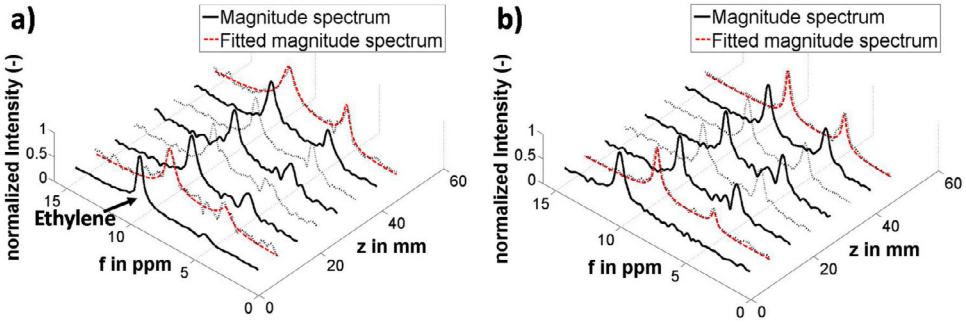

Fig. 3. Magnitude spectra measured in (a) the sponge catalyst support and (b) the honeycomb catalyst support at the same voxel position along the longitudinal axis of the reactor. The measured magnitude spectra were normalized by their maximum value and plotted alternating with solid and dashed lines for better readability. Additionally each second and last spectrum of the diagrams are shown with the corresponding MPM-fitted magnitude spectrum superimposed (red). The spectra were acquired at reaction conditions of the configuration "low flow rate" (cf. Table 1). (For interpretation of the references to colour in this figure legend, the reader is referred to the web version of this article.)

To quantify the volumetric fraction of ethylene and ethane, the maximum number of signals was set to two (ethylene, ethane). This was appropriate because the hydrogen signal of H_2 gas was not detected due to its very short transverse relaxation time. In each voxel, the number of signals was automatically determined (0, 1 or 2) to account for voxels with low signal-to-noise ratio (SNR) (e.g., outside the reactor) or regions where ethane was not or not yet produced. The amplitudes determined by the MPM algorithm were assigned to their corresponding chemical component on the basis of the associated frequency. The ethane/ethylene ratio was determined by normalizing the amplitudes to the number of attached hydrogen atoms per molecule and dividing the normalized amplitudes. This procedure was chosen to avoid unnecessary integration errors, particularly for regions with broad resonance lines where signal overlap may lead to an overestimation of the smaller component.

The MRSI data sets of this study were processed using in-house developed IDL (Interactive Data Language, version 7.0, Exilis Visual Information Solutions, Bolder, USA) and Matlab (version 7.11.0, The MathWorks, Inc., Natick, USA) programs.

2.4. Modeling approach

For the simulations, we used a pseudo homogeneous 1D fixed bed reactor model that combines the fluid and solid phase into a single effective phase and thus neglects interfacial heat and mass transfer. Neglecting interfacial mass transfer in this case is justified because of the Mears' criterion calculated in the Appendix (cf. Appendix A Supplementary data). Furthermore, based on the temperature measurements, we assume isothermal conditions for the low flow rate experiment. In addition, pressure is considered to be constant because of the short reactor and high gas permeabilities of the catalyst supports. Consequently, an overall mass balance and n species mass balances are necessary to describe the process with sufficient physical accuracy. The balance equations read:

$$\frac{dG}{dz} = 0 \tag{1}$$

$$G\frac{d\omega_i}{dz} = M_i \sum_{j=1}^{n_r} \nu_{ij}\eta_j r_j^{(V)},\ i = 1\ldots n_s \tag{2}.$$

Here $G = \rho e v_z$ describes the gas load, which remains constant along the catalyst bed due to mass conservation. It is a product of the fluid density ρ, the porosity of the catalyst bed ε, and the longitudinal fluid velocity v_z. ω_i refers to the mass fraction, M_i to the molar weight, η_i to the effectiveness factor and ν_i to the stoichiometric coefficient of the respective component i. n_r is the number of species of the reaction system. The effectiveness factor η_i, accounting for mass transport limitations within the porous catalyst, is considered to be unity because of the thin catalyst layers on the supports (approximately 6 μm and 20 μm for honeycomb and sponge, respectively, cf. Appendix A in Supplementary data) and the low temperatures (see estimation of the Thiele modulus in Appendix A in Supplementary data). The balance equations were subject to Dirichlet boundary conditions:

$$G(z=0) = G_0 \tag{3} \text{ and}$$

$$\omega_i(z=0) = \omega_{i,0} \tag{4}$$

where 0 indicates inlet conditions.

The density is calculated from the ideal gas law:

$$\rho = \frac{pM}{R_u T}. \tag{5}$$

Here, R_u is to the universal gas constant and T the temperature of the system.

An explicit expression for the reaction rate $r_j^{(V)}$ was derived from kinetic data from the literature. For the occurring reaction conditions the expression for the reaction rate was assumed to follow a power rate law:

$$r^{(Site)} = A\exp\left\{-\frac{E_a}{R_u T}\right\}\left(p_{H_2}^m p_{C_2H_4}^n\right), \tag{6},$$

where $r^{(Site)}$ is the reaction rate per active surface site of the catalyst, A is the pre-exponential factor, and E_a is the activation energy of the catalyst. Since the partial pressure of ethylene, p_{C2H4}, was much higher than 7 kPa during all experiments, the reaction order of ethylene m was set to zero [25]. The expression for the rate equation (Eq. (6)) was then fitted to kinetic data published in [19], wherein the reaction order or the partial pressure of hydrogen, p_{H2}, was found to be 1.18 ± 0.2 and $E_a = (37 \pm 0.63)$ kJ/mol (cf. Fig. S1). These values are in good agreement with other data from literature [25].

The pre-exponential factor A could not be derived from the kinetic data due to uncertainties regarding the quantity of active sites of the catalysts investigated in [19]. Hence, A was adapted to the MRSI results shown in Section 3.2. Note that, due to the adaption, the pre-exponential factor A might not only account for collision frequency and the probability of matching orientation of the reactant molecules, but could in principle also account for mass transport within the washcoat. Nevertheless, the estimation of the effectiveness factor η_i (cf. Appendix A in Supplementary data) indicates that this macro kinetic effect is negligible.

Assuming that the amount of catalyst, m_{Pt}, is homogeneously distributed on the catalyst surface, the active site related reaction rate, Eq. (6), was used to calculate the volumetric reaction rate by

relating the amount of catalyst to the total volume of the catalyst bed V_{tot}, and the molar weight M_{Pt}:

$$r^{(V)} = r^{Site}\frac{m_{Pt}}{V_{tot}M_{Pt}} \quad (7)$$

The system of differential equations of the 1D model was solved numerically using well established integration libraries [26,27]. The pre-exponential factor A was determined by minimizing the difference between the experimental and model results in a root-mean-square sense [28].

3. Results and discussion

Due to the axial resolution of the 3D MRSI method 22 slices could be utilized to track the reaction progress along the catalyst bed. Eight typical normalized magnitude spectra measured on the sponge and the honeycomb are shown in Fig. 3a and b, respectively. The spectra originate from the same voxel position along the longitudinal axis of the reactor.

Both sets of spectra profiles follow the same pattern: In the first spectra no or just insignificant amounts of ethane were detected. The ethane signal then increases along the first half of the reactor length and subsequently remains stable at the last three to four spectra. To demonstrate the performance of the applied fit routine (cf. Section 2.3), the second and last spectrum of the diagrams are shown with superimposed MPM-fitted magnitude spectra.

In accordance with former NMR studies [17] on ethylene hydrogenation a significant shift of the positions of the spectral peaks could not be observed with one exception: The ethylene peak of the first spectra of Fig. 3a and b is shifted by up to 2 ppm compared to the other ethylene peaks. This might result from B_0 changes, due to the transition between pure gas and catalytic monolith, which should be located there. The elevated SNR of the first spectra compared to the following spectra supports this explanation because of the higher signal from voxels with free gas compared to voxels containing also solid material.

The comparably small peak width of all observed spectra implies that the NMR signal primarily arises from the ethylene and ethane molecules of the gas phase and not from surface-adsorbed molecules. For comparison, spectra of an adsorbed and free gas ethylene/ethane mixture are shown in Fig. S2. This assumption is supported by the comparably high SNR variation in Fig. 3a (sponge) compared to Fig. 3b (honeycomb): The material of the honeycomb is significantly more permeable to gas than the struts of the Al_2O_3 sponge (cf. Fig. 4a and Fig. 5a). Thus in spectra, which are measured in voxels with a high amount of solid material, like sponge struts, the amount of detectable gas is lower, hence the SNR decreases, and this may reduce both precision and accuracy of spectrum analysis (cf. second and fourth spectrum in Fig. 3a). However, this effect of SNR decrease allows for deducing macroscopic morphological properties of gas impermeable catalyst support structures (cf. Fig. 4b).

3.1. Spatially resolved gas concentration analysis

The results of the spatially resolved gas MRSI analysis demonstrate that the NMR patterns match the porous structures of the investigated catalytic supports. Due to its macroscopic dimensions, the analysis of the sponge packing enables to detect the position and shape of the macro pores and structure depending reaction zones, whereas the analysis of the honeycomb (600 cpsi) allows for conclusions concerning the overall reaction process and the distribution of the catalytic coating.

Fig. 4a shows a photographic image of the cross section of the sponge packing. The cross section was located at the interface between the second and the third sponge segment of the catalytic sponge packing (z = 32 mm, cf. Fig. 1a). A corresponding NMR image is shown in Fig. 4b. This image of ethylene was measured by MRSI during a constant flow of a non-reactive mixture of ethylene and argon. For the sake of comparability with Fig. 4a, the gray scale of Image 4b was inverted, i.e., black represents high signal intensity and white low signal intensity. The comparison of Fig. 4a and b demonstrates that the macroscopic morphology of the sponge can be determined by MRSI at flow conditions. Significant pore structures, which are shown in Fig. 4a, are also clearly recognizable in Fig. 4b. The glass casing of the catalyst bed is also delineated in Fig. 4b, marked by a bright ring, which surrounds the sponge cross section. The gray ring shaped area which surrounds the glass casing, results from ethylene molecules that permeate the gap filled by the sealing cord between glass casing and reactor wall (cf. Fig. 2).

Fig. 4c and d show the resulting ethane concentration maps of the low and high flow rate experiments, respectively (cf. Table 1). The concentration maps were calculated based on the ethane/ethylene ratio determined from the 3D MRSI data as well as the inlet and outlet conditions. The procedure is described in detail in [17]. The concentration pattern corresponds to the position of the pores. Thus the reaction product is mainly detectable in areas with a high share of pore volume.

In comparison with Fig. 4c the concentration distribution within the pores of Fig. 4d appears to be more heterogeneous. This can be explained by the different reaction conditions (cf. Table 1): Due to the increase of flow velocity in the high flow rate experiment, the residence time is decreased and the process shown in Fig. 4d has not reached its maximum conversion at that position (cf. Fig. 6). Hence the gas molecules inside the sponge packing are not evenly distributed within all pores of the sponge, and areas with higher and lower reactivity are still distinguishable.

In order to compare the results of the sponge packing with the honeycomb experiments, Fig. 5a shows a photographic image of the honeycomb cross section and Fig. 5b shows an NMR image of ethylene measured during a constant flow of a non-reactive mixture of ethylene and argon. Fig. 5c and d depict ethane concentration maps of the low (Fig. 5c) and high flow rate experiments (Fig. 5d) at z = 32 mm, respectively. Note that in Fig. 5b, the grayscale was not inverted, i.e., white corresponds to high signal intensity.

In contrast to Fig. 4a and b, the macroscopic structures of the honeycomb are not visible in the MR image shown in Fig. 5b. The signal intensity is homogenously distributed within the cross section of the honeycomb. The reasons for this are twofold: On the one hand the cordierite honeycomb is permeable to gas, thus gas molecules inside the ceramic structures of the honeycomb produce an NMR signal and the signal intensity is not significantly lowered there. On the other hand the cells of the honeycomb are too small to be sufficiently resolved using the present MRSI voxel size. Future MRSI studies with improved spatial resolution will require stronger phase encoding gradients, which may cause technical problems due to the limited maximum gradient strength and signal distortions by gradient induced eddy currents. The alternative use of a longer phase encoding period will increase the delay between RF excitation and signal detection, thus leading to SNR losses, particularly for rapidly decaying time domain signals which correspond to broad resonance lines. Higher spatial resolution, i.e., a reduced voxel size, will also decrease the inherent SNR, which could be compensated for by a longer total measurement time (averaging) and/or improved RF coil design.

In accordance with the NMR image of Fig. 5b, the concentration distribution of ethane shown in Fig. 5c and d appears nearly homogenous. Just a slight decrease of ethane concentration toward the centre of the honeycomb is noticeable. This might be an indication of a lower amount of catalytic material in the central areas compared to the outer areas of the coated monolith, due to an inhomogeneous wetting of the monolith during the coating pro-

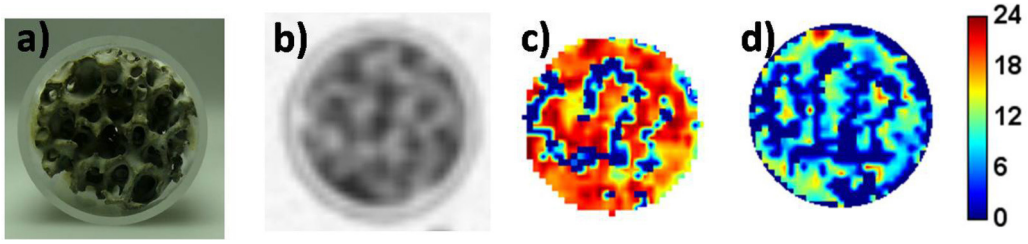

Fig. 4. (a) Photographic image of the cross section of the catalytic sponge packing at z = 32 mm. (b) NMR ethylene image (with inverted greyscale) of the cross section of the catalytic sponge packing at z = 32 mm measured by 3D MRSI during a constant flow of a non-reactive mixture of ethylene and argon. (c) Volumetric ethane concentration map of the low flow rate experiment of the catalytic sponge packing at z = 32 mm (d) Volumetric ethane concentration map of the high flow rate experiment of the catalytic sponge packing at z = 32 mm. All concentrations are given in vol%.(For interpretation of the references to colour in this figure legend, the reader is referred to the web version of this article.)

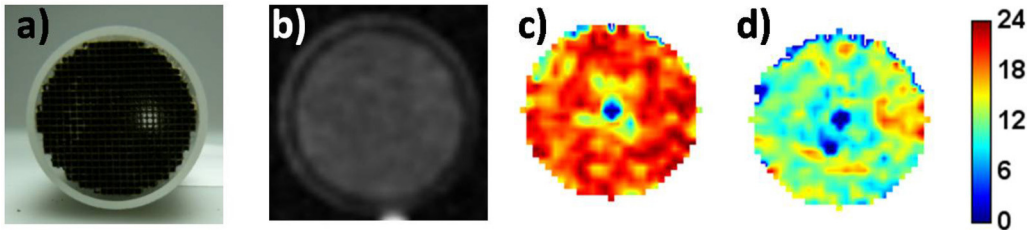

Fig. 5. (a) Photographic image of the cross section of the honeycomb catalyst (b) NMR ethylene image of the cross section of the honeycomb catalyst at z = 32 mm measured by 3D MRSI during a constant flow of a non-reactive mixture of ethylene and argon. (c) Volumetric ethane concentration map of the low flow rate experiment of the honeycomb catalyst at z = 32 mm (d) Volumetric ethane concentration map of the high flow rate experiment of the honeycomb catalyst at z = 32 mm. All concentrations are given in vol%.(For interpretation of the references to colour in this figure legend, the reader is referred to the web version of this article.)

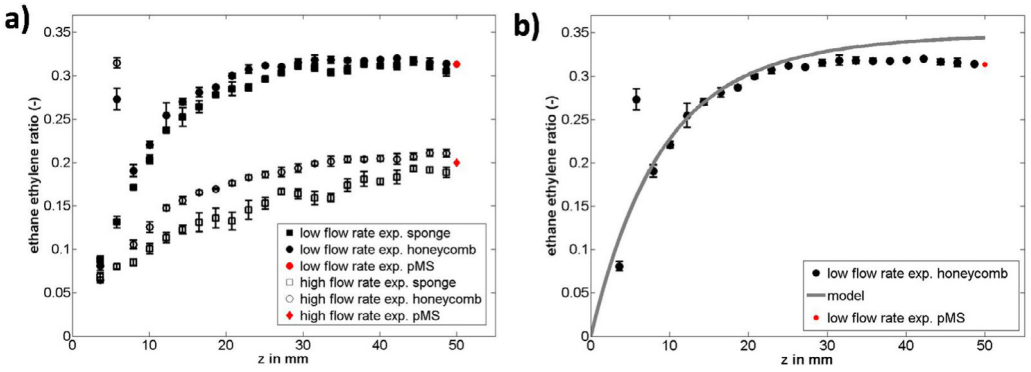

Fig. 6. (a) Ethane/ethylene ratio profiles of the experiments of this study. The standard deviation was calculated on the basis of the three individual measurements. The outliers of the honeycomb profiles are caused by measurement artifacts as described in the text. (b) Ethane/ethylene ratio profile of the low flow rate experiment catalyzed by the honeycomb with superimposed model of the reaction process.

cedure. Furthermore, no ethane appears to occur in a small area in the centre of the cross section. The apparent lack of ethane is caused by a failure of the fit algorithm, which occurs because artifact signals superimpose the ethylene and ethane signals in the respective areas. The artifact signals may originate from local contamination of the honeycomb. This would also explain the more frequent occurrence of that error in Fig. 5d, since the influence of local contamination is exacerbated by a low SNR.

3.2. MRSI measurement and simulation of the reaction progress

To further investigate the reaction progress along the longitudinal axis of the reactor, the SNR of the MRSI data sets was increased by repeating every experiment three times and adding the time domain signals before performing the fitting procedure. To determine the mean ethane/ethylene ratio of each slice, the amplitudes of each signal were added, and then the ethane/ethylene ratio was calculated from the combined amplitude values. These ethane/ethylene ratios were plotted over the longitudinal position of the slices (cf. Fig. 6a). The applied averaging process has the advantage, that porosity depending SNR variations do not influence the outcome.

The profiles of the low flow rate experiment of both investigated catalyst beds show a characteristic degressive pattern: After a strong ethane concentration gradient at the beginning of the catalyst beds, the profile flattens and levels at maximum conversion at two-thirds of the length of the catalyst bed and then remains stable until the end of the catalyst bed. The outlier at $z \approx 6$ mm of the honeycomb profile are caused by disturbing artifact signals. The localized artifact signals in this slice, which was also observed in the high flow rate experiment of the honeycomb, appeared at the same frequency range as the ethane signal. Both signals added up and caused a reproducible overestimation of the ethane/ethylene ratio in that slice. Note that the ethane/ethylene ratio measured by MRSI at the end of the catalyst bed is in a very good agreement with the ethane/ethylene ratio calculated from the pMS measurements.

Furthermore, the profiles measured at low flow rate are nearly identical for both catalyst supports, which indicates that the differ-

ent support structures do not influence the process performance significantly. Further it leads to the assumption that differing convectional transport has an insignificant impact on the reaction progress of both reaction systems. The temperature differences between the inlet and the outlet of both catalyst beds support this assumption: The difference for both experiments is about 10 K. The observed temperature difference between the inlet and outlet temperature of the sponge packing and the honeycomb can also be due to a slightly different position of the ethylene glycol capsules: The gap between the uncoated cordierite segments and the coated honeycomb was ca. 1–2 mm wider compared to the experimental set up of the sponge packing.

The profiles of the high flow rate experiments differ more considerably: Compared to the profile of the honeycomb support the profile of the sponge packing is less degressive, the maximum conversion is reached only at the end of the catalyst bed. In addition, the outlet temperatures of both experiments differ by more than 10 K, while the inlet temperatures are nearly identical. It is worth to point out that in both experiments the final conversions determined by either MRSI or pMS measurements are in good agreement.

The differences compared to the low flow rate experiments are unlikely the result of different mass transport limitations (cf. Appendix A in Supplementary data), but rather indicate an enhanced influence of convection. Under consideration of the isobaric reaction conditions and the same flow rate in both setups, the gas load within both catalyst beds should be constant. The sponge packing, however, has a higher amount of struts per volume element compared to the honeycomb. This would lead to an increased gas flow velocity within the sponge packing and thus to a decrease of contact time of the gas molecules, which could cause the flatting of the ethane/ethylene ratio profile. In addition, the increased flow velocity would move the reaction zone somewhat further to the outlet.

To prove the physical plausibility of the 3D MRSI measurements, the model introduced in Section 2.4 was used to simulate the ethylene hydrogenation process and the results were compared with the findings of the MRSI measurements. A well known problem of validating simulation approaches with experimental data is accurate knowledge of the boundary conditions of a process. Therefore, the low flow rate experiment of the honeycomb was chosen to validate the simulation approach. The temperature boundary conditions were assumed to be nearly isothermal, because on the one hand the temperature difference between the inlet and the outlet is comparably low. On the other hand the concentration gradients are quite low across the cross section of the catalyst bed (cf. Fig. 5c, Fig. S3). However, the occurring concentration gradients appear to be more localized. In addition, the NMR signal intensity profiles indicate that there are only minor temperature differences between the central and boundary areas of the catalyst bed (cf. Fig. S4). Accordingly, the applied 1D simulation approach should be adequate to provide reasonable results.

The model used for simulation (cf. Eq. (1)–(7)) was not completely deterministic and required a fitting of the pre-exponential factor (set to $1.7794\,10^{-22}$ mol s^{-1} $Pa^{-1.18}$) to the experimental data (cf. Fig. 6b). The simulation shows the same degressive pattern as the MRSI derived ethane/ethylene ratio profiles. Model and experimental data diverge slightly at the end of the catalyst bed. The deviation between model and experimental data is below 10% and can at least partly be explained by slightly different flow conditions between model and experiment: While in the model all of the reactant gases flow through the catalyst bed and nearly all of the hydrogen is converted, in the experiment a small share of the reactant gases permeates through the sealing cord (cf. Fig. 2) and is not available for the catalytic reaction. This small amount of not converted hydrogen was also detected by the pMS at the outlet (cf. Table 1) and lead to somewhat reduced ethane/ethylene ratios compared to the model. In addition, in the simulation the reaction process is assumed to be completely isothermal, while in the experiments some temperature gradients along the catalyst bed are very likely to occur. These diverging boundary conditions are also a source for discrepancies between model and experimental data.

However, despite the deviations between model and experimental data at the end of the catalyst bed and the necessary adjustment of the kinetic model, the simulation underlines physical plausibility of the experimental data and forms the basis for future investigations.

In the high flow rate experiments, no reliable assumptions for boundary conditions could be made due to considerable temperature differences between the inlet and the outlet. The determination of the boundary conditions of these experiments is still an open question and will be subject of future studies.

Regarding the applicability of 3D MRSI for characterizing catalyzed gas reactions in larger model reactors, a number of aspects have to be considered. The gas molecules should give rise to NMR signals at different chemical shifts to enable signal separation. To achieve a sufficient SNR, a compromise is required between the spatial resolution, the measurement time and the gas concentration. Furthermore, optimized NMR pulse sequences (with ultrashort echo time) and NMR hardware components (e.g., high static magnetic field, strong and rapidly switchable magnetic field gradients, efficient RF coils) are required. In general, data quality will also depend on the properties of the applied catalyst supports and the detected gases (relaxation times), and will be reduced with increasing temperature and flow velocity. The construction of NMR compatible reactors is another critical issue, particularly for studies at high temperature and high pressure. Because of the large number of factors, a detailed analysis of the applicability of MRSI is required for each specific model reactor.

4. Conclusion

An optimized 3D MRSI method has been successfully developed to non-invasively map the concentration distribution inside different monolithic catalysts using the ethylene hydrogenation under different reaction conditions as an example. The measured concentrations at the outlet are in remarkably good agreement (deviations below 5%) with simultaneously performed mass-spectrometric measurements. Furthermore, the qualitative development of the reaction progress was confirmed by comparing the measured concentration profiles with a 1D model of the reactor, which was based on kinetic data from the literature. Minor deviations between model and experimental data could be explained by differing flow and boundary conditions between experiment and simulation.

However, more efforts should be made to employ the 3D MRSI method not only for measuring spatially resolved gas concentrations but also to determine temperature fields to describe the reaction process more comprehensively [14], and thus validate simulation approaches for various reaction conditions.

In conclusion, the presented study demonstrates the feasibility of measuring spatially resolved concentration maps of a gas phase process non-invasively within different opaque and mechanically inaccessible monolithic catalyst supports. Thus, information from 3D MRSI can provide the basis to develop and validate more complex modeling approaches, which will allow a deeper insight into the interactions between catalyst, catalyst support and gas phase, thus helping to identify potentials for enhancements of process performances.

Acknowledgements

We would like to thank BASF Catalyst Germany GmbH, Nienburg and Roswita Krebs-Goldbecker from the glass workshop of the University of Bremen. This work was in part supported by the German Research Foundation (DFG) within the Research Training Group GRK 1860 "Micro-, meso- and macroporous nonmetallic Materials: Fundamentals and Applications" (MIMENIMA).

Appendix A. Supplementary data

Supplementary data associated with this article can be found, in the online version, at http://dx.doi.org/10.1016/j.cattod.2016.02.062.

References

[1] R. Heck, S. Gulati, R. Farrauto, Chem. Eng. J. 82 (2001) 149.
[2] E. Tronconi, G. Groppi, C. Visconti, Curr. Opin. Chem. Eng. 5 (2014) 55.
[3] I. Gräf, G. Ladenburger, B. Kraushaar-Czarnetzki, Chem. Eng. J. 287 (2016) 425.
[4] M. Hettel, C. Diehm, B. Torkashvand, O. Deutschmann, Catal. Today 216 (2013) 2.
[5] T. Schildhauer, K. Pangarkar, J. van Ommen, J. Nijenhuis, J. Moulijn, F. Kapteijn, Chem. Eng. J. 185–186 (2012) 250.
[6] D. Vervloet, F. Kapteijn, J. Nijenhuis, J. van Ommen, Chem. Eng. J. 233 (2013) 265.
[7] I. Koptyug, Magnetic resonance imaging methods in heterogeneous catalysis, in: J. Yarwood, R. Douthwaite, S. Duckett (Eds.), Spectroscopic Properties of Inorganic and Organometallic Compounds, Vol. 45, The Royal Society of Chemistry, 2014, 2016, p.1.
[8] I. Koptyug, A. Lysova, A. Kulikov, V. Kirillov, V. Parmon, R. Sagdeev, Appl. Cata. A: Gen. 267 (2004) 143.
[9] L. Gladden, M. Mantle, A. Sederman, Adv. Catal. 50 (2006) 1.
[10] A. Lysova, I. Koptyug, A. Kulikov, V. Kirillov, R. Sagdeev, Top. Catal. 52 (2009) 1371.
[11] C. Jameson, Chem. Rev. 91 (1991) 1375.
[12] P. Glover, P. Mansfield, Rep. Prog. Phys. 65 (2002) 1489.
[13] L.-S. Bouchard, S. Burt, M. Anwar, K. Kovtunov, I. Koptyug, A. Pines, Science 319 (2008) 442.
[14] N. Jarenwattananon, S. Glöggler, T. Otto, A. Melkonian, W. Morris, S. Burt, O. Yaghi, L.-S. Bouchard, Nature 502 (2013) 537.
[15] A. Moulé, M. Spence, S.-I. Han, J. Seeley, K. Pierce, S. Saxena, A. Pines, Proc. Natl. Acad. Sci. U. S. A. 100 (2003) 9122.
[16] J. Seeley, S.-I. Han, A. Pines, J. Magn. Reson. 167 (2004) 282.
[17] J. Ulpts, W. Dreher, M. Klink, J. Thöming, Appl. Cata. A: Gen. 502 (2015) 340.
[18] H. Ebrahimi, H. Shaghaghi, M. Tafazzoli, Concepts Magn. Reson. Part A 38A (2011) 269.
[19] R.D. Cortright, S. Goddard, J. Rekoske, J. Dumesic, J. Catal. 127 (1991) 342.
[20] T. Dorling, M. Eastlake, R. Moss, J. Catal. 14 (1969) 23.
[21] J. Schlatter, M. Boudart, J. Catal. 24 (1972) 482.
[22] Y. Hua, T. Sarkar, IEEE Trans. on 38 (1990) 814.
[23] Y.-M. Wang, H. Lee, D.V. Apte, Int. J. Imaging Syst. Technol. 4 (1992) 201.
[24] Y.-Y. Lin, P. Hodgkinson, M. Ernst, A. Pines, J. Magn. Reson. 128 (1997) 30.
[25] G. Bond, Metal-Catalysed Reactions of Hydrocarbons, Springer Science + Business Media Inc., 2005.
[26] A. Hindmarsch, in: R. Stepleman (Ed.), A Systematized Collection of Ode Solvers, Scientific Computing, North-Holland, Amsterdam, 1983, p. 55.
[27] L. Kiewidt, J. Thöming, Chem. Eng. Sci. 132 (2015) 59.
[28] S. Nocedal, Numerical Optimization, Springer, New York, USA, 2006.